Article

Scale-Up of a Heterogeneous Photocatalytic Degradation Using a Photochemical Rotor−Stator Spinning Disk Reactor

Arnab Chaudhuri,[§] Stefan D. A. Zondag,[§] Jasper H. A. Schuurmans, John van der Schaaf,* and Timothy Noël*

Cite This: https://doi.org/10.1021/acs.oprd.2c00012

Read Online

ACCESS | 📊 Metrics & More | 📖 Article Recommendations | 🆘 Supporting Information

ABSTRACT: Many chemical reactions contain heterogeneous reagents, products, byproducts, or catalysts, making their transposition from batch to continuous-flow processing challenging. Herein, we report the use of a photochemical rotor−stator spinning disk reactor (pRS-SDR) that can handle and scale solid-containing photochemical reaction conditions in flow. Its ability to handle slurries was showcased for the TiO_2-mediated aerobic photodegradation of aqueous methylene blue. The use of a fast rotating disk imposes high shear forces on the multiphase reaction mixture, ensuring its homogenization, increasing the mass transfer, and improving the irradiation profile of the reaction mixture. The pRS-SDR performance was also compared to other lab-scale reactors in terms of water treated per reactor volume and light power input.

KEYWORDS: *heterogeneous photochemistry, flow chemistry, rotor−stator spinning disk reactor, photodegradation, scale-up, solid handling*

INTRODUCTION

In recent years, photon-induced transformations have received an upsurge in attention from both academia and industry due to the popularity of photocatalysis.[1] Advances in LED technologies,[2] the need for sustainable chemistry[3,4] and continued efforts to develop and scale up photochemical processes by embracing continuous-flow processing[5−13] have resulted in a myriad of different reactor designs to bridge the gap between academia and industry. Ranging from the numbering up of micro- and millireactors to the design of completely novel reactor types, the productivities of photochemical reactors have seen tremendous growth over the past years.[14−16]

Despite these important advances, one key issue remains challenging for large-scale continuous-flow photochemical reactions, that is, the clogging problems associated with solid handling, both for the use of solid reactants/catalysts and the generation of solids during operation. Oftentimes, this results in the development of alternative homogeneous systems when shifting from batch to continuous processing, for example, by swapping heterogeneous bases or photocatalysts with homogeneous alternatives.[17] Apart from the additional efforts required to realize this heterogeneous-to-homogeneous shift, the reaction selectivity can be affected and downstream processing often becomes more cumbersome (e.g., separation and recovery of the homogeneous photocatalyst or byproducts).

The field of solid handling and slurry processing in the continuous manufacturing of chemicals is therefore of major interest to enable the transition from the laboratory scale to industrial fine-chemical production.[18] Solid particles can be kept in suspension via active or passive solid-management techniques.[19,20] For example, active solid particle agitation in flow can be achieved by stirring (e.g., continuous stirred-tank reactors[21−23]), ultrasonic irradiation,[24−27] and oscillatory/

pulsation flow,[28] whereas passive techniques can use static mixing elements or flow-induced agitation (e.g., secondary vortices in multiphase flow regimes).[29,30] Combinations of active and passive elements have also been reported, such as the merger of static mixing elements and pulsation flow observed in the HANU reactor concept.[28,31−33]

Another technology which holds promise for solid/slurry handling in flow is the rotor−stator spinning disk reactor (RS-SDR) (Figure 1A). This reactor type can generate a high degree of shear and turbulence in the reaction mixture from the rotation of a disk (∼130 mm in diameter) in a narrow rotor−stator gap, either using a thin film or in dispersed operation mode. As a consequence, high mass[34−40] and heat transfer[41,42] rates have been reported for the spinning disk reactor system, which in turn have been used to intensify a number of chemical reactions/processes.[43−47] An application of this reactor, adapted to enable homogeneous irradiation of the dispersed reaction mixture, has been recently published by our groups for an intensified photochemical gas−liquid process.[48] In this paper, we demonstrate that the photochemical RS-SDR (pRS-SDR) in its dispersed operation mode can be exploited for the handling of solid-containing heterogeneous photochemical systems.

As a suitable benchmark reaction, we selected the photocatalytic degradation of organic dyes, which are problematic to remove from wastewater effluents using conventional purification methods (Figure 1B).[49−51] For this application, semi-
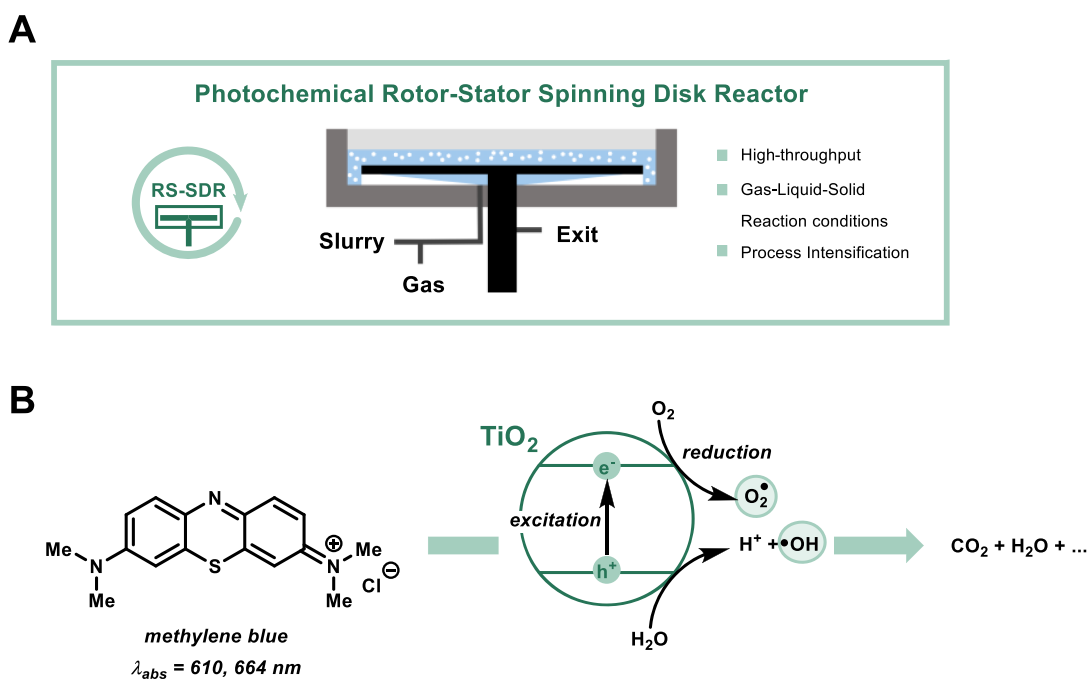
Figure 1. Photocatalytic degradation of MB using TiO_2 photocatalysis in a pRS-SDR. (A) pRS-SDR enables scale-up of complex heterogeneous photocatalytic reaction conditions. (B) Degradation of MB enabled by titanium dioxide semiconductor photocatalysis.

conductors are often used as recoverable heterogeneous photocatalysts; a typical example being titanium dioxide (TiO_2) due to its chemical stability, nontoxic nature, low cost, and high photocatalytic activity.[52,53] The electron–hole pairs generated upon the excitation of TiO_2 can produce reactive radicals (so-called reactive oxygen species, Figure 1B), which nonselectively oxidize the organic pollutants, such as methylene blue (MB), to carbon dioxide, water, and various mineralization products.[50,54−56] Interestingly, the photodegradation of organic dyes using TiO_2 has been extensively researched over the years and has served as a benchmark reaction for novel reactor designs, ranging from laboratory to intermediate scales and from batch to continuous-flow operation modes.[57−65] An additional advantage of this transformation is the possibility of easily assessing the remaining concentration of MB using conventional UV–vis spectroscopical tools. In this work, we report on the ability of the pRS-SDR to process complex aqueous gas–liquid–solid reaction streams without clogging and demonstrate that high productivity rates can be obtained for the TiO_2-mediated aerobic photodegradation of aqueous MB. We have also evaluated this photodegradation experimentally in a batch reactor and compared the pRS-SDR and batch reactor with other reactor types in the literature.

■ EXPERIMENTAL SECTION

General Information. Solutions with the desired concentration of MB (10 ppm) were made using demineralized water as the solvent, and a certain amount of TiO_2 (Evonik Aeroxide P25, 21 nm) was added. Gaseous O_2 was supplied with a mass flow controller (Bronkhorst EL-FLOW) and set to the desired flow rate. The samples taken from the reaction mixture were first diluted with ethanol before the solid particles were filtered using a syringe filter (CHROMAFIL Xtra PTFE 0.2 μm). The use of ethanol was also necessary to remove any adsorbed MB on the TiO_2 into the analyte. Analysis of the samples was done

using a spectrophotometer (UV-2501PC). A calibration curve was made at $\lambda = 657$ nm (see the Supporting Information, Figures S1 and S2) and was used to obtain the conversion of MB.

Batch Setup. The batch setup employed in our work is schematically shown in the Supporting Information (Figure S4). Inside a 3D-printed cylindrical vessel, an LED strip was attached (365 nm UV, 60 W maximum input power, see the Supporting Information, Figure S3, for emission spectrum). This strip was connected to an external power supply, which could regulate its power input. To keep a constant power per volume during the experiments, the power was adjusted after taking a sample to account for the decrease in volume. The vial (Pyrex, 7.5 mL) containing the reaction mixture (4 mL) was placed inside the photochemical vessel through the lid, and oxygen was supplied via a needle placed in the reaction mixture. Mixing occurred via a magnetic stirrer at a fixed position for all experiments. The reactor was air-cooled to maintain the reaction mixture at room temperature.

pRS-SDR Setup. The construction of the reactor setup for visible-light photochemistry has been previously reported.[48] The relevant internal dimensions of the reactor are given here for completeness. The rotor has a diameter of 130 mm, the distance between the rotor and stators is kept to 2 mm, and the total volume of the reactor is 64 mL, where the irradiated volume makes up 27 mL. However, due to the use of UV-A light, the setup was covered to shield the operator from harmful irradiation. On top of the reactor, the cover containing the light source was placed (Figure 6). The used light source was an LED floodlight placed on a mount (365 nm UV, 175 W maximum input power, see the Supporting Information, Figure S3, for the emission spectrum). The cover was constructed by the Equipment and Prototype Center at the TU Eindhoven and was made of stainless steel and insulation materials. The top part also holds a fan, allowing for extra cooling, in addition to the heat sink of the light source. The electrical system is

supplied with a fuse, so the system automatically shuts down in case of overheating.

The suspension was fed with a peristaltic pump (Masterflex Ismatec) and combined with the O_2 flow before entering the reactor via a T-mixer (reactor setup schematically shown in the Supporting Information, Figure S5). The vessel containing the suspension was covered from light and stirred continuously. The temperature was monitored at the outlet of the reactor using a thermocouple, and the temperature rise was typically no higher than 8 °C at steady state. For each data point, two samples were taken after at least three residence times to ensure a steady state.

■ RESULTS AND DISCUSSION

To investigate the photodegradation of aqueous MB, experiments were first performed using a small-scale batch reactor. The reaction with MB is particularly interesting since the aqueous solution gradually loses its bright blue color upon degradation and can be followed spectroscopically.[66] The presence of an oxidant (e.g., oxygen and hydrogen peroxide) that reacts with the excited electron in the conduction band of TiO_2 is of great importance since this can prevent the electron−hole recombination of the excited photocatalyst.[67] In this study, oxygen (O_2) was chosen, resulting in a triphasic gas−liquid−solid reaction system.

Photodegradation in Batch. Initially, control experiments were carried out in the absence of TiO_2, but with exposure to UV irradiation at the highest input power, to investigate the effect and significance of the direct photolysis pathway (Figure 2).[68] This experiment does result in some minor MB degradation, but its extent is negligible relative to the photocatalytic pathway, where full conversion is observed within 5 min of reaction time. Additionally, another control experiment without light irradiation but with the photocatalyst was conducted. In the absence of light irradiation, the adsorption of MB on the photocatalyst is noticeable but does not result in any MB degradation.

Next, the dependencies of the reaction rate on light intensity, TiO_2 concentration, and O_2 bubbling rate were investigated. A first-order reaction rate in the concentration of
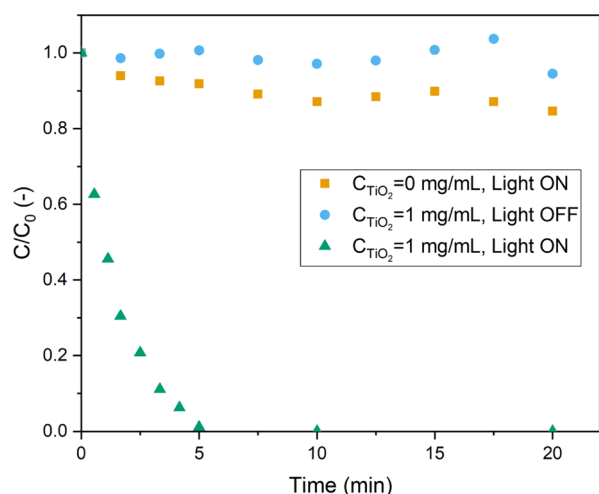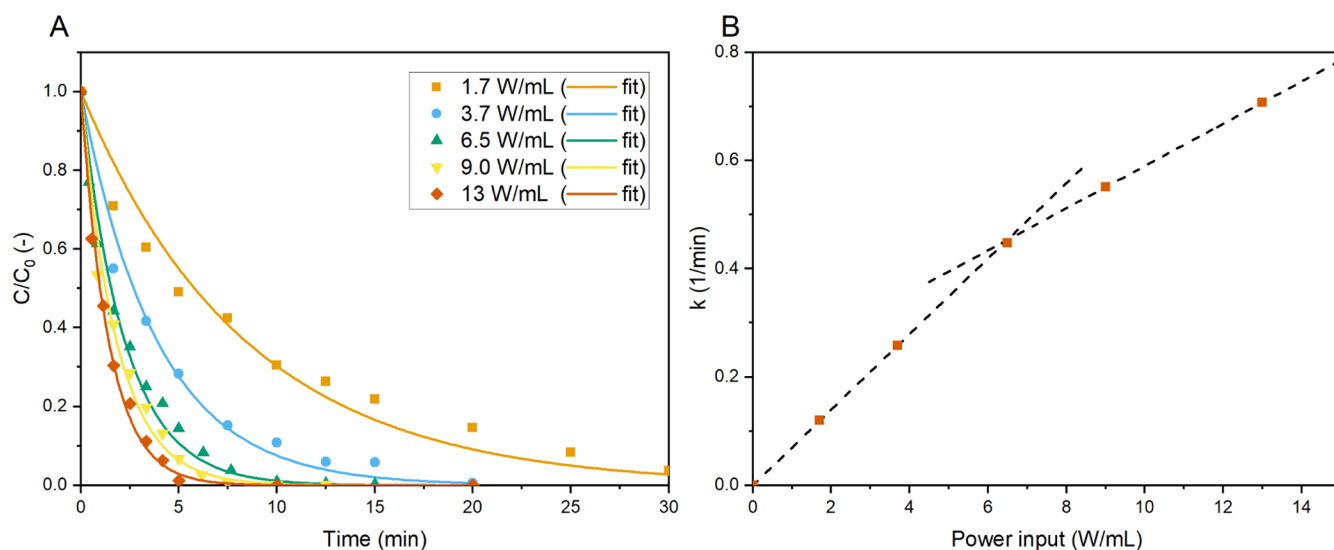
MB was found to approximate the overall photocatalytic system well (eq 1), where the apparent overall reaction rate constant (k) encompasses all other factors influencing the reaction rate (e.g., mass transfer and light attenuation).

$$\frac{dC_{MB}}{dt} = -kC_{MB} \tag{1}$$

We commenced with varying the power input of the UV LED strip using an external power supply to set the effective light intensity irradiating the sample. In Figure 3, the normalized MB concentrations for various power inputs per volume in time are given. Higher light intensities clearly enhance the reaction rate, where the apparent reaction rate constant for 13 W/mL (0.71 1/min) is almost sixfold compared to the one at 1.7 W/mL (0.12 1/min). However, the relation of the apparent reaction rate constant to the input power was found only to be linear for the additional intensity at lower power inputs (for <6.5 W/mL, see Figure 3B). This indicates a possible shift away from a fully photon-limited system, causing other factors to become more limiting.[6] Extension of the operating regime where higher light intensities result in faster degradation could possibly be achieved by intensifying mass transfer or by operating at increased concentration of the light-absorbing species, that is, the photocatalyst TiO_2.

Next, the photocatalyst concentration was varied while maintaining the irradiation at a power input of 6.5 W/mL. This was done for the ease of comparison with the continuous-flow setup (see the Supporting Information), where this is the maximum power input with the current configuration. Increasing the catalyst concentration increases the concentration of the light-absorbing species, allowing more photons to be absorbed. However, a too high concentration can also result in a nonhomogeneous irradiation and lead to additional irradiation losses caused by light scattering. Therefore, an optimal catalyst concentration was expected and found at 0.33 mg/mL (k = 0.48 1/min, see Figure 4). Notably, the previously used value of 1.0 mg/mL yielded a comparable rate constant (k = 0.45 1/min), while for higher and lower catalyst concentrations, the rate constant significantly dropped. Importantly, the suspension remained stable at relatively long time intervals: even at the highest catalyst concentration, no sedimentation of particles was observed at the bottom of the reactor.

Evaluation of the gas−liquid mass transfer effects in batch was done by varying the oxygen flow rate bubbled through the reaction mixture. These experiments were again conducted at a power input of 6.5 W/mL and the experimentally determined optimal catalyst concentration of 0.33 mg/mL. The flow rate of oxygen was varied from 0 to 10 mL/min, where at 0 mL/min, the headspace above the reaction mixture was O_2. The batch system could not be described well for flow rates other than 4 mL/min by the apparent first-order reaction kinetics, but the fitted curves are still shown and used to get an approximation of the reaction constants (Figure 5). The data shows that the oxygen flow rate influences the kinetic rate in a complicated way. At zero flow, it is evident that the oxygen saturation level of the mixture is sufficient to convert all the MB, although oxygen mass transfer may become the rate-limiting step at high conversions. Adding a bubble flow maintains a high-enough oxygen concentration to have MB as the rate-limiting reactant. The optimal flow rate was found to be 4.0 mL/min. At lower flow rates, the gas-to-liquid (G/L) mass transfer could be

Figure 2. Normalized concentration of MB vs time. The behavior in absence of UV irradiation or the catalyst is compared to the presence of both ([light power input 52 W (13 W/mL), 10 ppm MB, and 4.0 mL/min O_2 bubbling].

c

Figure 3. Normalized concentration of MB (A) apparent overall reaction constants (B) vs the time for different UV LED power inputs per volume with their fitted first-order concentration−time curves (10 ppm MB, C_{TiO_2} = 1.0 mg/mL, and 4.0 mL/min O_2 bubbling).
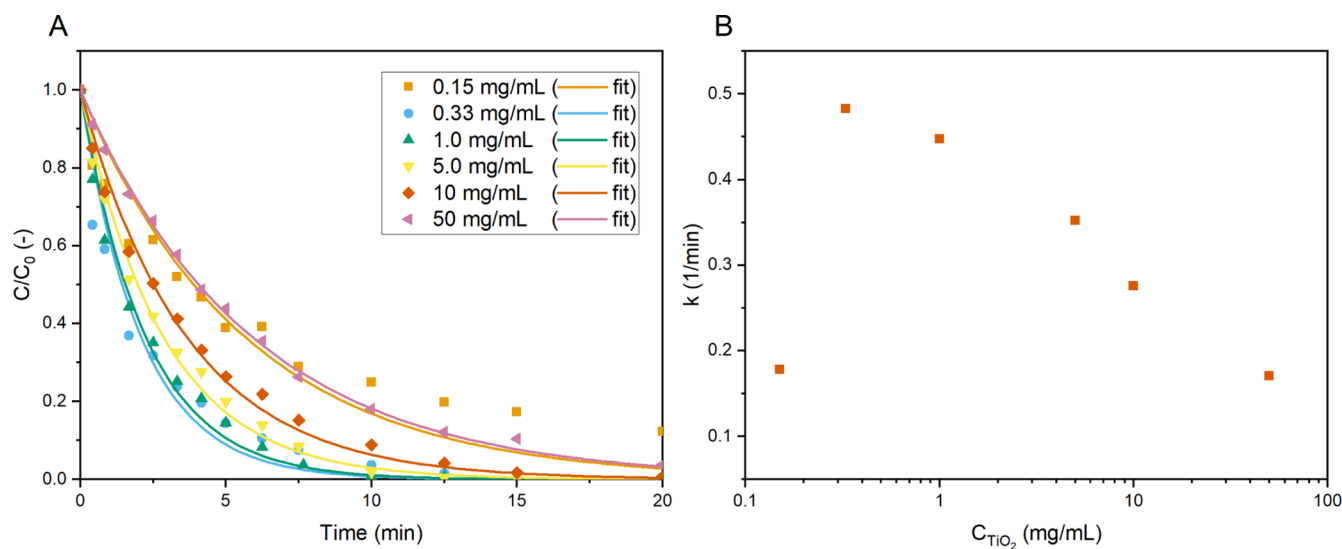
Figure 4. Normalized concentration of MB (A) and the apparent overall reaction constants (B) vs the time for varying catalyst concentrations [light input power 26 W (6.5 W/mL), 10 ppm MB, and 4.0 mL/min O_2 bubbling].

limiting the reaction rate, where the surface available for G/L mass transfer is not sufficient. It should also be noted that the gas bubbling also contributes to additional mixing of the reaction mixture. At flow rates higher than 4.0 mL/min, the formed bubbles appear larger in size, resulting in shorter contact times (due to higher bubble rise velocities) and could increase irradiation losses caused by scattering and transmission.

Photodegradation in the pRS-SDR. After investigation of the photodegradation of MB in batch, our research focus shifted toward the use of the pRS-SDR (schematically shown in Figure 6).

For multiphase continuous-flow processes, the liquid volume in the reactor is determined by the G/L ratio of the feed[48] and the solid volume fraction. The residence time in the pRS-SDR is relatively independent of the rotation as the differences in holdup are typically small for varying rotation speeds.[34,35,48,69] The rotation speed directly affects the mixing and mass transfer, effectively decoupling the mass transfer from the flow

rate or residence time, which distinguishes spinning disk reactors from nonagitated flow reactors. A relatively high catalyst concentration of 10 mg/mL (∼1.0 w % of the suspension) was chosen for the standard conditions in order to illustrate the ability of the pRS-SDR to handle high solid concentrations. The volumetric G/L ratio was generally kept at 1:1 to ensure an excess of O_2.

Initially, the liquid flow rate ($\Phi_{V,L}$) was varied while keeping the G/L ratio constant at 1:1 (Figure 7). The degradation of MB was enhanced drastically by increasing the rotation speed. This may be caused by an increase in liquid−solid and gas−liquid mass transfer, by increasing the dispersion of gas and solids in the liquid, by breaking up solid agglomerations, and/or by the reduction of the bubble size, allowing for more efficient gas−liquid mass transfer. Notably, the mixing efficiency reduces the light-penetration limitations we observed in the batch reactor as the reactants and catalyst are continuously replenished at the high-irradiation zones of the reactor, that is, at the quartz window. We have also estimated
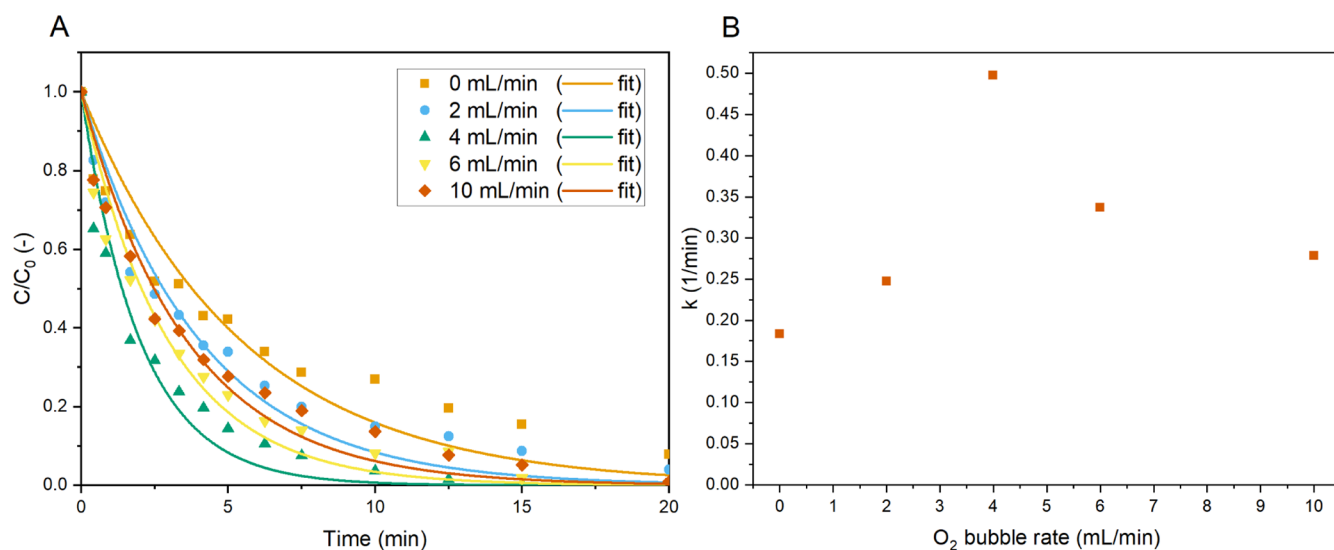
Figure 5. Normalized concentration of MB (A) and the apparent overall reaction constants (B) vs the time for different O_2 bubbling flow rates [light input power 26 W (6.5 W/mL), 10 ppm MB, and C_{TiO_2} = 0.33 mg/mL].
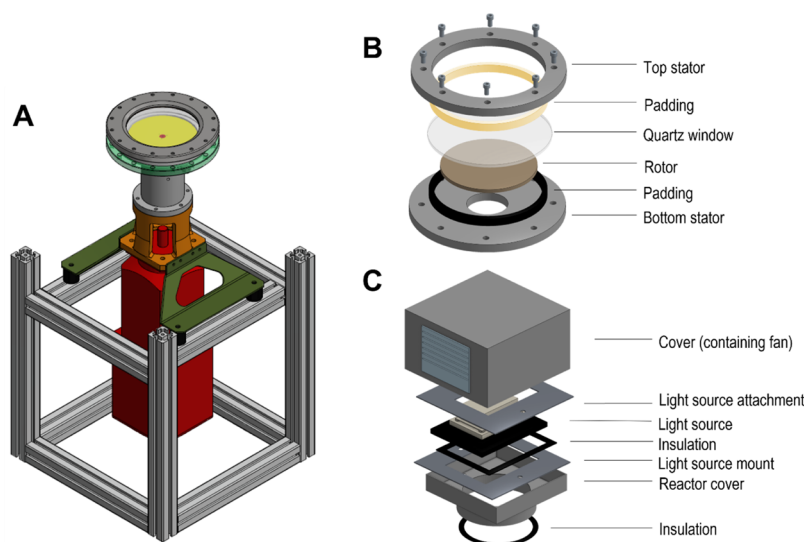

Figure 6. Schematic representation of the pRS-SDR. (A) Schematic of a fully assembled reactor without the cover. (B) Exploded view of the reactor. (C) Exploded view of the cover for the UV light source.

the resulting average k value (please see the Supporting Information for calculation details) in the pRS-SDR at 250 rpm (k = 0.061 1/min) and at 1500 rpm (k = 70 1/min) for the flow rate of 16.5 mL/min. This analysis clearly indicates the improvement in reaction rate due to an improvement in mixing. For comparison, the highest k value observed at the same light intensity (6.5 W/mL) in batch was k = 0.5 1/min. Of course, as Figure 7 also indicates, increasing the liquid flow rate and effectively decreasing the liquid residence time, leads to an increase in concentration of the remaining MB at the reactor outlet.

Next, the G/L ratio was increased to 3:1 and this situation was compared with a 1:1 ratio at a constant liquid flow rate (13.5 mL/min, see the Supporting Information, Figure S10). With a 3:1 G/L ratio, higher conversions could be reached at lower rotation speeds compared to a 1:1 G/L, suggesting the existence of gas−liquid mass transfer limitation of oxygen. At higher rotation speeds (∼1000 rpm), this effect diminished and both G/L ratios reached full degradation of MB. Further

investigation of the G/L ratio was performed by varying $\Phi_{V,L}$ at the highest rotation speed of 2000 rpm to ensure the best possible mixing and mass transfer. Two sets of experiments were performed, with the gas flow rates ($\Phi_{V,G}$) being kept constant at two separate values (Figure 8). For the constant gas flow rate of 13.5 mL/min, the maximum observed liquid flow rate that resulted in >90% MB degradation was found to be 19.5 mL/min. This yielded the best reactor performance thus far. We have used this value for the comparison between various reactor designs in the next section. No significantly different behavior is found at the higher gas flow rate, even though the performance at especially the higher liquid flow rates starts to worsen slightly. This might be attributed to an increase in the gas holdup, effectively lowering the liquid residence time.

Increasing the TiO_2 loading can increase the total amount of active sites and thus the adsorption of substrates. However, a higher TiO_2 loading results simultaneously in increased light scattering and light attenuation, limiting the maximum
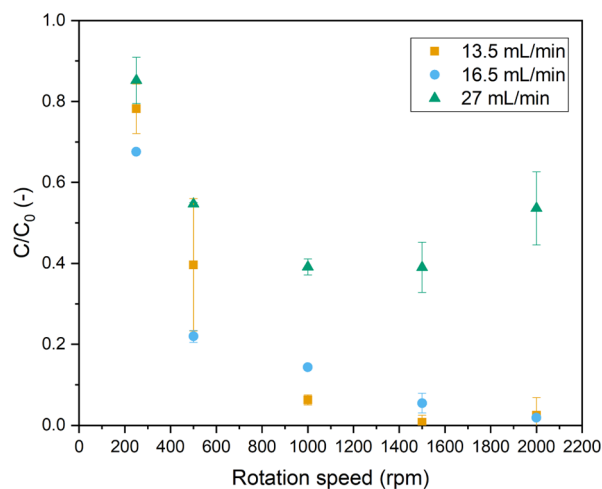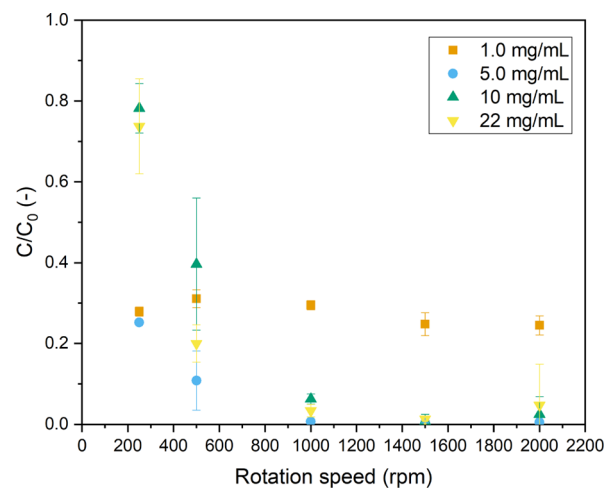
Figure 7. Normalized concentration of MB vs rotation speed for different flow rates, with a G/L ratio of 1:1 [light input power 175 W (6.5 W/mL), 10 ppm MB, and C_{TiO_2} = 10 mg/mL].
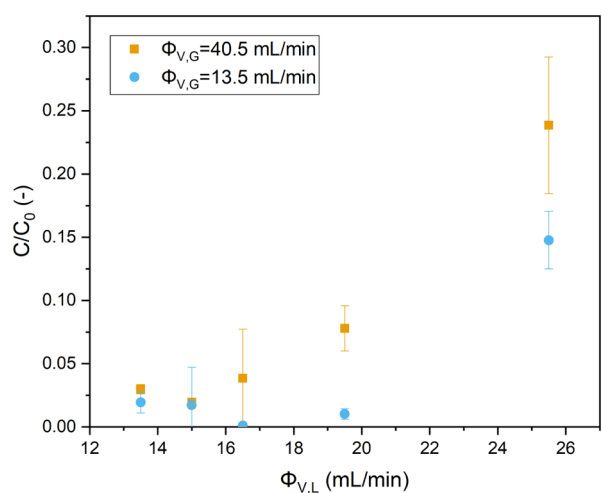
Figure 8. Normalized concentration of MB vs the liquid flow rate for two different constant gas flow rates at 2000 rpm [light input power 175 W (6.5 W/mL), 10 ppm MB, and C_{TiO_2} = 10 mg/mL].

observed reaction rate. Several catalyst concentrations have been screened at a liquid flow rate of 13.5 mL/min and a G/L ratio of 1:1. The results in Figure 9 show that for the investigated concentrations, only in the case of 1.0 mg/mL, full MB degradation cannot be reached, even at elevated rotation speeds. For all other catalyst loadings, increasing the rotation speed directly translates into higher conversions. This implies that for the higher catalyst loadings, the higher rotation speeds can overcome light penetration limitations (more opaque reaction solution due to higher heterogeneity). At higher rotation speeds, it can be expected that the solid catalysts are better dispersed in solution, leading to a higher fraction of surface area being available for the reaction. These factors in combination with improvements in mass transfer (solid−liquid and gas−liquid) are the most likely cause for the enhancements observed within the pRS-SDR.

Since almost all catalyst concentrations in Figure 9 reach full conversion around 1000 rpm, the liquid residence time was further decreased by doubling the liquid flow rate to 27.0 mL/min (while keeping the G/L ratio constant at 1:1). Under these reaction conditions, full conversion will not be reached,

Figure 9. Normalized concentration of MB vs rotation speed for different catalyst concentrations/loadings [light input power 175 W (6.5 W/mL), $\Phi_{V,L}$ = 13.5 mL/min, G/L ratio 1:1, 10 ppm MB.

which would allow us to identify practical limitations at higher catalyst loadings. Figure 10 shows indeed that full degradation of MB was not reached. However, the conversion improves consistently at increasing rotation speeds, even for catalyst concentrations as high as 45 mg/mL. Notably, no issues with the handling of this concentrated slurry were encountered during reactor operation (see the Supporting Information).

Reactor Comparison. In this section, the batch reactor and the pRS-SDR are compared to other reactor types for the TiO_2-enabled photodegradation of MB. Table 1 gives an overview of the reactor types, conditions, and performance of these reactors. Our work is compared to two reactor types using an immobilized photocatalyst and two reactor types operated under slurry conditions. The systems are benchmarked in two different ways to calculate the productivity. The first one is the amount of polluted water treated per unit of time per reactor volume, corrected for the power input of the light source (relative productivity I). Since this number can favor reactors with a very low reactor volume and a low-power
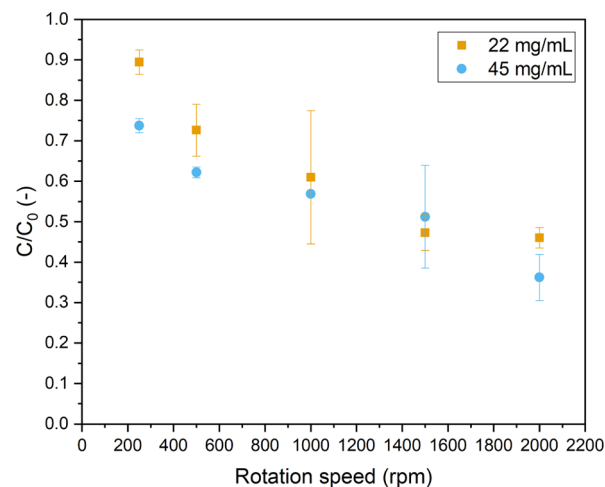
Figure 10. Normalized concentration of MB vs rotation speed for higher catalyst concentrations to test the limitations of the system [light input power 175 W (6.5 W/mL), $\Phi_{V,L}$ = 27 mL/min, G/L ratio 1:1, 10 ppm MB.

Table 1. Comparison of Some Reactor Types Used for the Photodegradation of MB Using TiO$_2$[a]

reactor type	TiO$_2$ usage	MB (ppm)	light input power and wavelength	reactor volume (mL)	reaction time (min)	relative productivity I[b]	relative productivity II[c]	source
thin-film spinning disk	immobilized	10	20 W 254 nm	~0.09	>167	0.073	2.54×10^{-4}	71
annular reactor	immobilized	8	20 W 254 nm	201	120	0.10	0.75	72
batch reactor	suspension C_{TiO2} = 2.5 mg/mL	2.1	125 W 340 nm	20	120	0.016	0.25	68
CPC reactor	suspension C_{TiO2} = 0.4 mg/mL	10	60 W 365 nm	600	>180	0.022	0.50	73
batch reactor (this work)	suspension C_{TiO_2} = 0.33 mg/mL	10	26 W 365 nm	4	10	0.74	0.14	
pRS-SDR (this work)	suspension C_{TiO_2} = 10 mg/mL	10	175 W 365 nm	27	<1.4[d]	1	1	

[a]The productivities do not take into account the initial MB concentrations of the treated water. [b]Water flow treated (mL/s) per reactor volume (mL) per light power input (W). Normalized to the pRS-SDR: 6.9×10^{-5} 1/(s·W). [c]Water flow treated (mL/s) per light power input (W). Normalized to the pRS-SDR: 1.9×10^{-3} mL/(s·W). [d]This is the liquid residence time at an assumed gas holdup of 0%, making this the maximum possible residence time. Gas holdups of <20% are expected.[48]

light source, this is considered not entirely suitable for scale-up investigations. Therefore, the reactors are also evaluated in terms of the amount of water treated per power of the light source and per unit of time (relative productivity II).

The pRS-SDR has the best performance for both comparison methods. It should be noted that the immobilized designs make use of a light source of 254 nm, which is more expensive and increases the effect of direct photolysis. The compound parabolic collector (CPC) reactor displays good performance at low catalyst concentrations. However, handling higher concentrations led to a decrease in the reactor performance, making this reactor type less suitable for subsequent process intensification and scale-up. A disadvantage of the pRS-SDR is that the rotor-induced mixing will lead to additional energy losses, which have not been accounted for in Table 1. This energy dissipation will increase with increasing rotation speed, where the amount of energy dissipated is estimated to be 37 W at 2000 rpm (accounting for <20% of the total power consumption).[70] Therefore, it is vital to optimize the reaction system so that the excess energy dissipated by the rotor translates to an increase in productivity.

The pRS-SDR shows excellent performance for the photodegradation and, most importantly, encountered no issues with solid handling. For the investigated catalyst concentrations, light penetration issues can actively be overcome by tuning the rotation speed of the rotor. The ability to increase mass transfer and obtain excellent mixing would also allow for process intensification, where concentrations of the reactants and catalyst can be increased together with the power of the light source. It should also be noted that the reactor system has not yet been fully optimized and, thus, the performance of the reactor can possibly be increased, for example, by using higher-intensity light sources.

CONCLUSIONS

Herein, the pRS-SDR was validated for continuous-flow heterogeneous photochemistry using the TiO$_2$-mediated

aerobic photodegradation of MB as a benchmark transformation. This high-shear photochemical reactor is uniquely suited to handle such complex solid-containing reaction mixtures and did not display any sign of reactor clogging, a problem often associated with other continuous-flow capillary reactors. The use of a fast rotating disk ensured homogenization of the reaction mixture, increased the mass transfer, and improved the irradiation profile of the reaction mixture. We anticipate that the pRS-SDR will aid in the transition from batch to continuous-flow operation in the pharmaceutical and agrochemical industry by facilitating the scale-up of challenging multiphase synthetic transformations.

■ ASSOCIATED CONTENT

ⓢ Supporting Information

The Supporting Information is available free of charge at https://pubs.acs.org/doi/10.1021/acs.oprd.2c00012.

Absorption and light source spectra, schematic batch and pRS-SDR reactor setups, overall reaction kinetics fitting methods, additional pRS-SDR behavior characteristics (e.g., extent of reactor fouling), and qualitative image analysis (PDF)

■ AUTHOR INFORMATION

Corresponding Authors

John van der Schaaf − Department of Chemical Engineering and Chemistry, Sustainable Process Engineering, Eindhoven University of Technology (TU/e), 5612 AZ Eindhoven, The Netherlands; ⓞ orcid.org/0000-0002-2856-8592; Email: j.vanderschaaf@tue.nl

Timothy Noël − Flow Chemistry Group, van't Hoff Institute for Molecular Sciences (HIMS), Universiteit van Amsterdam (UvA), 1098 XH Amsterdam, The Netherlands; ⓞ orcid.org/0000-0002-3107-6927; Email: t.noel@uva.nl

Authors

Arnab Chaudhuri − *Department of Chemical Engineering and Chemistry, Sustainable Process Engineering, Eindhoven University of Technology (TU/e), 5612 AZ Eindhoven, The Netherlands*

Stefan D. A. Zondag − *Flow Chemistry Group, van't Hoff Institute for Molecular Sciences (HIMS), Universiteit van Amsterdam (UvA), 1098 XH Amsterdam, The Netherlands;* orcid.org/0000-0003-1463-4867

Jasper H. A. Schuurmans − *Department of Chemical Engineering and Chemistry, Sustainable Process Engineering, Eindhoven University of Technology (TU/e), 5612 AZ Eindhoven, The Netherlands*

Complete contact information is available at:
https://pubs.acs.org/10.1021/acs.oprd.2c00012

Author Contributions

§Equal Contribution

Notes

The authors declare no competing financial interest.

■ REFERENCES

(1) Noël, T.; Zysman-Colman, E. The Promise and Pitfalls of Photocatalysis for Organic Synthesis. *Chem. Catal.* **2022**, DOI: 10.1016/j.checat.2021.12.015.

(2) Sender, M.; Ziegenbalg, D. Light Sources for Photochemical Processes − Estimation of Technological Potentials. *Chem.-Ing.-Tech.* **2017**, *89*, 1159−1173.

(3) Ravelli, D.; Dondi, D.; Fagnoni, M.; Albini, A. Photocatalysis. A Multi-Faceted Concept for Green Chemistry. *Chem. Soc. Rev.* **2009**, *38*, 1999−2011.

(4) Anastas, P. T.; Warner, J. C. *Green Chemistry: Theory and Practice*; Oxford University Press: New York, 1998.

(5) Van Gerven, T.; Mul, G.; Moulijn, J.; Stankiewicz, A. A Review of Intensification of Photocatalytic Processes. *Chem. Eng. Process.: Process Intensif.* **2007**, *46*, 781−789.

(6) Buglioni, L.; Raymenants, F.; Slattery, A.; Zondag, S. D. A.; Noël, T. Technological Innovations in Photochemistry for Organic Synthesis: Flow Chemistry, High-Throughput Experimentation, Scale-up, and Photoelectrochemistry. *Chem. Rev.* **2022**, *122*, 2752−2906.

(7) Di Filippo, M.; Bracken, C.; Baumann, M. Continuous Flow Photochemistry for the Preparation of Bioactive Molecules. *Molecules* **2020**, *25*, 356.

(8) Kayahan, E.; Jacobs, M.; Braeken, L.; Thomassen, L. C.; Kuhn, S.; Van Gerven, T.; Leblebici, M. E. Dawn of a New Era in Industrial Photochemistry: The Scale-up of Micro: The Mesostructured Photoreactors. *Beilstein J. Org. Chem.* **2020**, *16*, 2484−2504.

(9) Dong, Z.; Wen, Z.; Zhao, F.; Kuhn, S.; Noël, T. Scale-up of Micro- and Milli-Reactors: An Overview of Strategies, Design Principles and Applications. *Chem. Eng. Sci. X* **2021**, *10*, 100097.

(10) Rehm, T. H. Reactor Technology Concepts for Flow Photochemistry. *ChemPhotoChem* **2020**, *4*, 235−254.

(11) Loubière, K.; Oelgemöller, M.; Aillet, T.; Dechy-Cabaret, O.; Prat, L. Continuous-Flow Photochemistry: A Need for Chemical Engineering. *Chem. Eng. Process.: Process Intensif.* **2016**, *104*, 120−132.

(12) Beaver, M. G.; Zhang, E.-x.; Liu, Z.-q.; Zheng, S.-y.; Wang, B.; Lu, J.-p.; Tao, J.; Gonzalez, M.; Jones, S.; Tedrow, J. S. Development and Execution of a Production-Scale Continuous [2 + 2] Photo-cycloaddition. *Org. Process Res. Dev.* **2020**, *24*, 2139−2146.

(13) Lee, D. S.; Sharabi, M.; Jefferson-Loveday, R.; Pickering, S. J.; Poliakoff, M.; George, M. W. Scalable Continuous Vortex Reactor for Gram to Kilo Scale for UV and Visible Photochemistry. *Org. Process Res. Dev.* **2020**, *24*, 201−206.

(14) Wan, T.; Wen, Z.; Laudadio, G.; Capaldo, L.; Lammers, R.; Rincón, J. A.; García-Losada, P.; Mateos, C.; Frederick, M. O.; Broersma, R.; et al. Accelerated and Scalable C(Sp 3)−H Amination via Decatungstate Photocatalysis Using a Flow Photoreactor Equipped with High-Intensity LEDs. *ACS Cent. Sci.* **2022**, *8*, 51−56.

(15) Bottecchia, C.; Lévesque, F.; McMullen, J. P.; Ji, Y.; Reibarkh, M.; Peng, F.; Tan, L.; Spencer, G.; Nappi, J.; Lehnherr, D.; et al. Manufacturing Process Development for Belzutifan, Part 2: A Continuous Flow Visible-Light-Induced Benzylic Bromination. *Org. Process Res. Dev.* **2021**, DOI: 10.1021/acs.oprd.1c00240.

(16) Harper, K. C.; Zhang, E.-X.; Liu, Z.; Grieme, T.; Towne, T. B.; Mack, D. J.; Griffin, J.; Zheng, S.; Zhang, N.; Gangula, S.; et al. Commercial-Scale Visible Light Trifluoromethylation of 2-Chlor-othiophenol Using CF₃I Gas. *Org. Process Res. Dev.* **2022**, *26* (2), 404−412.

(17) Mazzarella, D.; Pulcinella, A.; Bovy, L.; Broersma, R.; Noël, T. Rapid and Direct Photocatalytic C(Sp³)−H Acylation and Arylation in Flow. *Angew. Chem., Int. Ed.* **2021**, *60*, 21277−21282.

(18) Hartman, R. L. Managing Solids in Microreactors for the Upstream Continuous Processing of Fine Chemicals. *Org. Process Res. Dev.* **2012**, *16*, 870−887.

(19) Flowers, B. S.; Hartman, R. L. Particle Handling Techniques in Microchemical Processes. *Challenges* **2012**, *3*, 194−211.

(20) Green, J.; Holdø, A.; Khan, A. A Review of Passive and Active Mixing Systems in Microfluidic Devices. *Int. J. Multiphys.* **2007**, *1*, 1−32.

(21) Pomberger, A.; Mo, Y.; Nandiwale, K. Y.; Schultz, V. L.; Duvadie, R.; Robinson, R. I.; Altinoglu, E. I.; Jensen, K. F. A Continuous Stirred-Tank Reactor (CSTR) Cascade for Handling Solid-Containing Photochemical Reactions. *Org. Process Res. Dev.* **2019**, *23*, 2699−2706.

(22) Harper, K. C.; Moschetta, E. G.; Bordawekar, S. V.; Wittenberger, S. J. A Laser Driven Flow Chemistry Platform for Scaling Photochemical Reactions with Visible Light. *ACS Cent. Sci.* **2019**, *5*, 109−115.

(23) Francis, D.; Blacker, A. J.; Kapur, N.; Marsden, S. P. Readily Reconfigurable Continuous-Stirred Tank Photochemical Reactor Platform. *Org. Process Res. Dev.* **2022**, *26*, 215−221.

(24) Dong, Z.; Zondag, S. D. A.; Schmid, M.; Wen, Z.; Noël, T. A Meso-Scale Ultrasonic Milli-Reactor Enables Gas−Liquid-Solid Photocatalytic Reactions in Flow. *Chem. Eng. J.* **2022**, *428*, 130968.

(25) Falß, S.; Tomaiuolo, G.; Perazzo, A.; Hodgson, P.; Yaseneva, P.; Zakrzewski, J.; Guido, S.; Lapkin, A.; Woodward, R.; Meadows, R. E. A Continuous Process for Buchwald−Hartwig Amination at Micro-, Lab-, and Mesoscale Using a Novel Reactor Concept. *Org. Process Res. Dev.* **2016**, *20*, 558−567.

(26) Horie, T.; Sumino, M.; Tanaka, T.; Matsushita, Y.; Ichimura, T.; Yoshida, J.-i. Photodimerization of Maleic Anhydride in a Microreactor without Clogging. *Org. Process Res. Dev.* **2010**, *14*, 405−410.

(27) Kuhn, S.; Noël, T.; Gu, L.; Heider, P. L.; Jensen, K. F. A Teflon Microreactor with Integrated Piezoelectric Actuator to Handle Solid Forming Reactions. *Lab Chip* **2011**, *11*, 2488−2492.

(28) Bianchi, P.; Williams, J. D.; Kappe, C. O. Oscillatory Flow Reactors for Synthetic Chemistry Applications. *J. Flow Chem.* **2020**, *10*, 475−490.

(29) Poe, S. L.; Cummings, M. A.; Haaf, M. P.; McQuade, D. T. Solving the Clogging Problem: Precipitate-Forming Reactions in Flow. *Angew. Chem., Int. Ed.* **2006**, *45*, 1544−1548.

(30) Peng, Z.; Wang, G.; Moghtaderi, B.; Doroodchi, E. A Review of Microreactors Based on Slurry Taylor (Segmented) Flow. *Chem. Eng. Sci.* **2022**, *247*, 117040.

(31) Debrouwer, W.; Kimpe, W.; Dangreau, R.; Huvaere, K.; Gemoets, H. P. L.; Mottaghi, M.; Kuhn, S.; Van Aken, K. Ir/Ni Photoredox Dual Catalysis with Heterogeneous Base Enabled by an

Oscillatory Plug Flow Photoreactor. *Org. Process Res. Dev.* **2020**, *24*, 2319−2325.

(32) Bianchi, P.; Williams, J. D.; Kappe, C. O. Continuous Flow Processing of Bismuth-Photocatalyzed Atom Transfer Radical Addition Reactions Using an Oscillatory Flow Reactor. *Green Chem.* **2021**, *23*, 2685−2693.

(33) Rosso, C.; Gisbertz, S.; Williams, J. D.; Gemoets, H. P. L.; Debrouwer, W.; Pieber, B.; Kappe, C. O. An Oscillatory Plug Flow Photoreactor Facilitates Semi-Heterogeneous Dual Nickel/Carbon Nitride Photocatalytic C−N Couplings. *React. Chem. Eng.* **2020**, *5*, 597−604.

(34) Meeuwse, M.; Lempers, S.; van der Schaaf, J.; Schouten, J. C. Liquid−Solid Mass Transfer and Reaction in a Rotor−Stator Spinning Disc Reactor. *Ind. Eng. Chem. Res.* **2010**, *49*, 10751−10757.

(35) Meeuwse, M.; van der Schaaf, J.; Kuster, B. F. M.; Schouten, J. C. Gas-Liquid Mass Transfer in a Rotor-Stator Spinning Disc Reactor. *Chem. Eng. Sci.* **2010**, *65*, 466−471.

(36) Meeuwse, M.; Hamming, E.; van der Schaaf, J.; Schouten, J. C. Effect of Rotor−Stator Distance and Rotor Radius on the Rate of Gas−Liquid Mass Transfer in a Rotor−Stator Spinning Disc Reactor. *Chem. Eng. Process.: Process Intensif.* **2011**, *50*, 1095−1107.

(37) Visscher, F.; van der Schaaf, J.; de Croon, M. H. J. M.; Schouten, J. C. Liquid−Liquid Mass Transfer in a Rotor−Stator Spinning Disc Reactor. *Chem. Eng. J.* **2012**, *185−186*, 267−273.

(38) Haseidl, F.; Pottbäcker, J.; Hinrichsen, O. Gas−Liquid Mass Transfer in a Rotor−Stator Spinning Disc Reactor: Experimental Study and Correlation. *Chem. Eng. Process.: Process Intensif.* **2016**, *104*, 181−189.

(39) de Beer, M. M.; Keurentjes, J. T. F.; Schouten, J. C.; van der Schaaf, J. Bubble Formation in Co-Fed Gas−Liquid Flows in a Rotor-Stator Spinning Disc Reactor. *Int. J. Multiphase Flow* **2016**, *83*, 142−152.

(40) Manzano Martínez, A. N.; Chaudhuri, A.; Assirelli, M.; van der Schaaf, J. Effects of Increased Viscosity on Micromixing in Rotor-Stator Spinning Disk Reactors. *Chem. Eng. J.* **2022**, *434*, 134292.

(41) de Beer, M. M.; Pezzi Martins Loane, L.; Keurentjes, J. T. F.; Schouten, J. C.; van der Schaaf, J. Single Phase Fluid-Stator Heat Transfer in a Rotor−Stator Spinning Disc Reactor. *Chem. Eng. Sci.* **2014**, *119*, 88−98.

(42) Kleiner, J.; Münch, B.; Rößler, F.; Fernengel, J.; Habla, F.; Hinrichsen, O. CFD Simulation of Single-Phase Heat Transfer in a Rotor-Stator Spinning Disc Reactor. *Chem. Eng. Process.: Process Intensif.* **2018**, *131*, 150−160.

(43) Zou, D.; Li, J.; Deng, J.; Jin, Y.; Chen, M. Continuous Preparation of Size-Controllable BaTiO$_3$ Nanoparticles in a Rotor−Stator Spinning Disk Reactor. *Ind. Eng. Chem. Res.* **2021**, *60*, 14511−14518.

(44) van Kouwen, E. R.; Winkenwerder, W.; Brentzel, Z.; Joyce, B.; Pagano, T.; Jovic, S.; Bargeman, G.; van der Schaaf, J. The Mixing Sensitivity of Toluene and Ethylbenzene Sulfonation Using Fuming Sulfuric Acid Studied in a Rotor-Stator Spinning Disc Reactor. *Chem. Eng. Process.: Process Intensif.* **2021**, *160*, 108303.

(45) Wang, Y.; Li, J.; Jin, Y.; Chen, M.; Ma, R. Extraction of Chromium (III) from Aqueous Waste Solution in a Novel Rotor-Stator Spinning Disc Reactor. *Chem. Eng. Process.: Process Intensif.* **2020**, *149*, 107834.

(46) Kleiner, J.; Hinrichsen, O. Epoxidation of Methyl Oleate in a Rotor-Stator Spinning Disc Reactor. *Chem. Eng. Process.: Process Intensif.* **2019**, *136*, 152−162.

(47) Chaudhuri, A.; Backx, W. G.; Moonen, L. L. C.; Molenaar, C. W. C.; Winkenweder, W.; Ljungdahl, T.; van der Schaaf, J. Kinetics and Intensification of Tertiary Amine N-Oxidation: Towards a Solventless, Continuous and Sustainable Process. *Chem. Eng. J.* **2021**, *416*, 128962.

(48) Chaudhuri, A.; Kuijpers, K. P. L.; Hendrix, R. B. J.; Shivaprasad, P.; Hacking, J. A.; Emanuelsson, E. A. C.; Noël, T.; van der Schaaf, J. Process Intensification of a Photochemical Oxidation Reaction Using a Rotor-Stator Spinning Disk Reactor: A Strategy for Scale Up. *Chem. Eng. J.* **2020**, *400*, 125875.

(49) Karpińska, J.; Kotowska, U. Removal of Organic Pollution in the Water Environment. *Water* **2019**, *11*, 2017.

(50) Wetchakun, K.; Wetchakun, N.; Sakulsermsuk, S. An Overview of Solar/Visible Light-Driven Heterogeneous Photocatalysis for Water Purification: TiO$_2$- and ZnO-Based Photocatalysts Used in Suspension Photoreactors. *J. Ind. Eng. Chem.* **2019**, *71*, 19−49.

(51) Cambié, D.; Bottecchia, C.; Straathof, N. J. W.; Hessel, V.; Noël, T. Applications of Continuous-Flow Photochemistry in Organic Synthesis, Material Science, and Water Treatment. *Chem. Rev.* **2016**, *116*, 10276−10341.

(52) Gaya, U. I.; Abdullah, A. H. Heterogeneous Photocatalytic Degradation of Organic Contaminants over Titanium Dioxide: A Review of Fundamentals, Progress and Problems. *J. Photochem. Photobiol., C* **2008**, *9*, 1−12.

(53) Kiselev, V. M.; Evstrop'ev, S. K.; Starodubtsev, A. M. Photocatalytic Degradation and Sorption of Methylene Blue on the Surface of Metal Oxides in Aqueous Solutions of the Dye. *Opt. Spectrosc.* **2017**, *123*, 809−815.

(54) Tayade, R. J.; Natarajan, T. S.; Bajaj, H. C. Photocatalytic Degradation of Methylene Blue Dye Using Ultraviolet Light Emitting Diodes. *Ind. Eng. Chem. Res.* **2009**, *48*, 10262−10267.

(55) Augugliaro, V.; Bellardita, M.; Loddo, V.; Palmisano, G.; Palmisano, L.; Yurdakal, S. Overview on Oxidation Mechanisms of Organic Compounds by TiO$_2$ in Heterogeneous Photocatalysis. *J. Photochem. Photobiol., C* **2012**, *13*, 224−245.

(56) Riente, P.; Noël, T. Application of Metal Oxide Semi-conductors in Light-Driven Organic Transformations. *Catal. Sci. Technol.* **2019**, *9*, 5186−5232.

(57) Yatmaz, H. C.; Wallis, C.; Howarth, C. R. The Spinning Disc Reactor − Studies on a Novel TiO$_2$ Photocatalytic Reactor. *Chemosphere* **2001**, *42*, 397−403.

(58) Thomson, C. G.; Lee, A.-L.; Vilela, F. Heterogeneous Photocatalysis in Flow Chemical Reactors. *Beilstein J. Org. Chem.* **2020**, *16*, 1495−1549.

(59) Zangeneh, H.; Zinatizadeh, A. A. L.; Habibi, M.; Akia, M.; Hasnain Isa, M. Photocatalytic Oxidation of Organic Dyes and Pollutants in Wastewater Using Different Modified Titanium Dioxides: A Comparative Review. *J. Ind. Eng. Chem.* **2015**, *26*, 1−36.

(60) Alhaji, M. H.; Sanaullah, K.; Khan, A.; Hamza, A.; Muhammad, A.; Ishola, M. S.; Rigit, A. R. H.; Bhawani, S. A. Recent Developments in Immobilizing Titanium Dioxide on Supports for Degradation of Organic Pollutants in Wastewater- A Review. *Int. J. Environ. Sci. Technol.* **2017**, *14*, 2039−2052.

(61) Singh, S. K.; Mishra, P. K.; Upadhyay, S. N. Recent Developments in Photocatalytic Degradation of Insecticides and Pesticides. *Rev. Chem. Eng.* **2021**, DOI: 10.1515/revce-2020-0074.

(62) Kanan, S.; Moyet, M. A.; Arthur, R. B.; Patterson, H. H. Recent Advances on TiO$_2$-Based Photocatalysts toward the Degradation of Pesticides and Major Organic Pollutants from Water Bodies. *Catal. Rev.* **2020**, *62*, 1−65.

(63) McCullagh, C.; Skillen, N.; Adams, M.; Robertson, P. K. J. Photocatalytic Reactors for Environmental Remediation: A Review. *J. Chem. Technol. Biotechnol.* **2011**, *86*, 1002−1017.

(64) Adams, M.; Campbell, I.; McCullagh, C.; Russell, D.; Bahnemann, D. W.; Robertson, P. K. J. From Ideal Reactor Concepts to Reality: The Novel Drum Reactor for Photocatalytic Wastewater Treatment. *Int. J. Chem. React. Eng.* **2013**, *11*, 621−632.

(65) Khositanon, C.; Deepracha, S.; Assabumrungrat, S.; Ogawa, M.; Weeranoppanant, N. Simple Fabrication of a Continuous-Flow Photocatalytic Reactor Using Dopamine-Assisted Immobilization onto a Fluoropolymer Tubing. *Ind. Eng. Chem. Res.* **2022**, *61*, 1322−1331.

(66) Junploy, P.; Phuruangrat, A.; Plubphon, N.; Thongtem, S.; Thongtem, T. Photocatalytic Degradation of Methylene Blue by Zn2SnO4-SnO2 System under UV Visible Radiation. *Mater. Sci. Semicond. Process.* **2017**, *66*, 56−61.

(67) Tseng, D.-H.; Juang, L.-C.; Huang, H.-H. Effect of Oxygen and Hydrogen Peroxide on the Photocatalytic Degradation of Mono-

chlorobenzene in Aqueous Suspension. *Int. J. Photoenergy* **2012**, *2012*, 1−9.

(68) Houas, A.; Lachheb, H.; Ksibi, M.; Elaloui, E.; Guillard, C.; Herrmann, J. M. Photocatalytic Degradation Pathway of Methylene Blue in Water. *Appl. Catal., B* **2001**, *31*, 145−157.

(69) Manzano Martínez, A. N.; Chaudhuri, A.; Besten, M.; Assirelli, M.; van der Schaaf, J. Micromixing Efficiency in the Presence of an Inert Gas in a Rotor−Stator Spinning Disk Reactor. *Ind. Eng. Chem. Res.* **2021**, *60*, 8677−8686.

(70) de Beer, M. M.; Keurentjes, J. T. F.; Schouten, J. C.; van der Schaaf, J. Engineering Model for Single-Phase Flow in a Multi-Stage Rotor−Stator Spinning Disc Reactor. *Chem. Eng. J.* **2014**, *242*, 53−61.

(71) Boiarkina, I.; Norris, S.; Patterson, D. A. Investigation into the Effect of Flow Structure on the Photocatalytic Degradation of Methylene Blue and Dehydroabietic Acid in a Spinning Disc Reactor. *Chem. Eng. J.* **2013**, *222*, 159−171.

(72) Boiarkina, I.; Norris, S.; Patterson, D. A. The Case for the Photocatalytic Spinning Disc Reactor as a Process Intensification Technology: Comparison to an Annular Reactor for the Degradation of Methylene Blue. *Chem. Eng. J.* **2013**, *225*, 752−765.

(73) Betancourt-Buitrago, L. A.; Vásquez, C.; Veitia, L.; Ossa-Echeverry, O.; Rodriguez-Vallejo, J.; Barraza-Burgos, J.; Marriaga-Cabrales, N.; Machuca-Martínez, F. An Approach to Utilize the Artificial High Power LED UV-A Radiation in Photoreactors for the Degradation of Methylene Blue. *Photochem. Photobiol. Sci.* **2017**, *16*, 79−85.